Heat transport in nonuniform superconductors

Caroline Richard and Anton B. Vorontsov
Department of Physics, Montana State University, Bozeman, Montana 59717, USA
(Received 11 May 2016; revised manuscript received 11 July 2016; published 4 August 2016)

We calculate electronic energy transport in inhomogeneous superconductors using a fully self-consistent nonequilibrium quasiclassical Keldysh approach. We develop a general theory and apply it to a superconductor with an order parameter that forms domain walls of the type encountered in the Fulde-Ferrell-Larkin-Ovchinnikov state. The heat transport in the presence of a domain wall is inherently anisotropic and nonlocal. The bound states in the nonuniform region play a crucial role and control heat transport in several ways: (i) they modify the spectrum of quasiparticle states and result in Andreev reflection processes and (ii) they hybridize with the impurity band and produce a local transport environment with properties very different from those in a uniform superconductor. As a result of this interplay, heat transport becomes highly sensitive to temperature, magnetic field, and disorder. For strongly scattering impurities, we find that the transport *across* domain walls at low temperatures is considerably more efficient than in the uniform superconducting state.

DOI: 10.1103/PhysRevB.94.064502

I. INTRODUCTION

Electronic heat transport is a powerful tool to explore the properties of the superconducting state. It is a bulk probe that encodes information about both the density of electronic states and the quasiparticle relaxation times. Heat conductivity experiments have been used extensively to study the structure and symmetries of the superconducting order parameter in many different compounds [1]. The low-temperature behavior of thermal conductivity is a signature of either the absence or presence of low-energy excitations [2]. It can also be used as a directional probe of the gap structure, since it depends on the velocity of the low-energy excitations. One can measure the anisotropy of thermal conductivity along different directions and identify the Fermi velocity vectors of nodal quasiparticles [3–5]. Another way to study the nodal structure is to observe the response of nodal excitations to a rotated magnetic field [1]. The external magnetic field modifies the density of states [6,7] and the quasiparticles scattering times [8–10]. The magnitude of these effects depends on the orientation of the magnetic field relative to the nodes of the order parameter and the direction of the heat flow [1].

The power of this technique, however, is also the reason why the interpretation of thermal transport measurements is a difficult task, since the density of states and transport time of quasiparticles may not be independently available. In this respect, experiment and theory must be employed together in the analysis of data for reaching definite conclusions. In uniform superconductors, heat conductivity has been investigated in great details, using several approaches: Boltzmann transport theory [11], Green's functions technique [12], and quasiclassical methods [2] that prompted a rapid development on the experimental side.

There is growing interest in using thermal transport to study nonuniform superconductors [13] and topological surface states [14–16]. However, from the theory side, little is known about the heat flow in the presence of a spatially varying order parameter. The challenge here is to understand how quasiparticles transport energy from one point to another when both the quasiparticle density of states and scattering mean-free path depend on both energy and position. Under these conditions, it is important to treat—on the same footing—Andreev particle-hole conversion processes in inhomogeneous regions [17] and scattering processes on impurities.

As a result, in nonuniform superconductors, calculation of heat transport is difficult and so far has been carried out only in two different approximations. In the strongly inhomogeneous situation, as in the case of periodic and moderately dense Abrikosov vortex lattice near H_{c2}, one can average over the vortex lattice unit cell [18,19], assuming the local formula relating the heat current to the temperature gradient, $\boldsymbol{j}_h(\boldsymbol{R}) = -\hat{\kappa}\ \boldsymbol{\nabla} T(\boldsymbol{R})$, to hold everywhere. In this approach, one can analyze the effects of disorder and magnetic field on the density of states, lifetime, and heat transport of spatially extended quasiparticles outside vortex cores [9,10]. In a very different setting, the heat transport through a pinhole supporting Andreev bound states (ABS) was investigated [20]. When a phase bias φ is applied across the pinhole, highly degenerate Andreev bound states [17] appear at subgap energies controlled by both φ and the transparency of the pinhole. The sudden temperature drop across the pinhole produces a local heat current that depends on the phase bias, $j_h = -\kappa(\varphi)\delta T$. The bound states lying at the subgap energy do not directly couple to the continuum of quasiparticles to transport heat. Nevertheless, their presence modifies the effective transparency of the pinhole for quasiparticles above the gap. In particular, for a pinhole with perfect transparency, the subgap bound states reduce locally the spectral weight of continuum states, which suppresses the heat flow, $\kappa(\varphi) < \kappa(0)$. By contrast, at low transparency, the ABS lie just below the gap edge and enhance heat conductivity, $\kappa(\varphi) > \kappa(0)$, due to a resonance with the continuum [20]. However, in topological insulator junctions, the zero energy ABS are topologically protected, preventing such resonance [16].

Both of these approaches have limited applicability. In the pinhole calculation, the sudden drop approximation means point-localized ABS and lack of impurity scattering effects. The averaging procedure, on the other hand, works well for high temperature and fields where vortices are dense, but less well at low temperatures and fields, and even worse with fully gapped superconductors. It relies on a presence of a significant number of spatially extended low-energy

quasiparticles, but has no way of including the contribution of localized vortex core states. An exact theoretical treatment of the thermal transport that simultaneously takes into account impurity scattering in a spatially varying order parameter landscape, the effects of spatially localized Andreev bound states, and a position-dependent density of states, is lacking. In this direction, we provide, in this paper, a basis for future explorations of general nonuniform superconducting configurations.

There are several important details that we include in a complete treatment of the problem. First, effects of the Andreev states localized in the inhomogeneous region are taken into account on the same footing with the effects of the impurities that also produce midgap Andreev states distributed throughout the sample. Both kind of bound states result in modifications in the quasiparticle spectrum and scattering time, and their interaction is important. Second, the broken translation and rotation symmetry that appear in systems with a spatially modulated order parameter in general result in additional "vertex corrections" to the transport lifetime [21,22]. Third, the mean-free paths of the quasiparticles can be longer than the coherence-length scale of the order parameter variations, thus invalidating the picture of a local equilibrium and local response even for small temperature gradients.

As a particular model for the inhomogeneous phase we consider a domain wall between two degenerate configurations of the order parameter, which changes sign across the wall, $\Delta(-\infty) = -\Delta(+\infty)$. We also consider more complicated configurations with a periodic collection of multiple domain walls. We enforce the order parameter modulation through boundary conditions on the edges of the sample, and self-consistently compute the profile of the domain walls and spatially dependent impurity self-energies. The domain walls have a width of several coherence lengths, and host highly degenerate zero-energy Andreev bound states. Such profile of the order parameter is a realization of Larkin-Ovchinnikov configuration of the speculative Fulde-Ferrell-Larkin-Ovchinnikov (FFLO) phase [23–25]. Building a theoretical understanding of the thermal conductivity in this phase is important for experimental attempts to detect spatial modulations of the order parameter using heat transport [13]. At this point, it is not known how anisotropic is the heat flow in the presence of the hypothetical FFLO domain wall structures in the order parameter. For example, the typical assumption is that the heat flow across the domains is strongly constricted due to the presence of the ABS that do not carry heat. We find that this is not, in fact, true, and the combination of impurity scattering effects with the spatially extended range of the bound states can produce both suppression and enhancement of thermal transport compared to the uniform state.

The organization of the paper is as follows. In Sec. II, we describe our model and relate it to the experimental measurement technique. In Sec. III, we develop the formalism to compute thermal transport in a nonuniform superconductor using the Keldysh quasiclassical approach and t-matrix treatment of disorder. The linear response is discussed in Sec. III A; in Sec. III B, we formulate the boundary conditions for the quasiclassical propagator amplitudes. We apply this technique to compute heat flow across a single domain wall

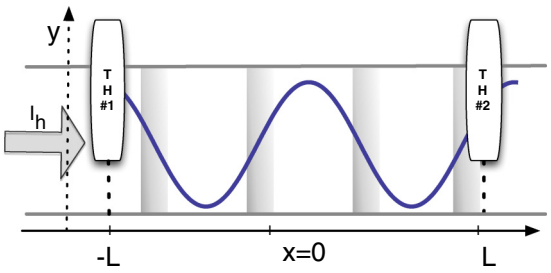

FIG. 1. A typical experimental setup for heat conductivity measurements involves establishing a steady-state current in the sample and measuring the effective local temperature T_1 and T_2. The heat conductance is defined as $\kappa = I_h \times 2L/(T_1 - T_2)$. We set a two-dimensional superconductor in the xy plane and for a given heat current I_h along the x axis we calculate the temperature difference between thermometers TH1 and 2 at $x = \pm L$. The sin line is a schematic representation of an FFLO modulation of the order parameter with shaded regions representing domain walls.

in Sec. IV A, and in Sec. IV B, we generalize it to the case of multiple domain walls and investigate the heat transport dependence on the number of domains, temperature, disorder, and spacing of domain walls. Finally, in Sec. IV C, we address the modifications arising from the Zeeman shifts of quasiparticle energies.

II. MODEL

We consider a spin-singlet superconductor with a quasi-two-dimensional cylindrical Fermi surface. Our model can be applied to both s- and d-wave superconductors, but we will focus on the case of a d-wave symmetry, for several reasons. First, most of the recent investigations of FFLO state have been done on materials with d-wave pairing, such as heavy-fermion [26] or organic [27] superconductors. Also, unconventional superconductors have a more general order parameter structure with low-lying nodal quasiparticles and are sensitive to disorder. We consider $\Delta(\hat{p}) \propto \cos 2(\phi_{\hat{p}} - \alpha)$ and present results for $\alpha = 0$, since we find that the particular value of α is not important.

Impurities are randomly distributed throughout the sample with concentration $c_{\rm imp}$. The impurity scattering potential is assumed pointlike and isotropic with amplitude u. The system is set out of equilibrium by introducing a thermal current flowing along the x axis. As the stationary state is reached, a temperature gradient builds up. We define the heat conductivity between two points as $\kappa = I_h \times 2L/(T_1 - T_2)$, where I_h is the stationary-state heat flow, and T_1 and T_2 are the local temperatures as if measured by two distant thermometers positioned at $x = \pm L$. Our goal is to compute the effective temperature bias $dT = T_1 - T_2$ for a given I_h, in the presence of spatially modulated order parameter as shown in Fig. 1.

III. THEORY

A convenient approach to study nonuniform superconductors out of equilibrium is the quasiclassical formulation of the Keldysh technique [28]. It is formulated in terms of the Green function $\hat{g}(\boldsymbol{R}, \hat{p}, \epsilon)$, which for stationary states depends on the

center of mass coordinate $\boldsymbol{R}$, the direction of the momentum on the Fermi surface $\hat{p}$, and the energy ϵ. It is an 8×8 matrix in particle-hole (Nambu), spin, and Keldysh space. In the Keldysh space, it is given by

$$\hat{g} = \begin{pmatrix} g^R & g^K \\ 0 & g^A \end{pmatrix}, \tag{1}$$

where the superscripts $R/A/K$ stand for Retarded, Advanced, and Keldysh. The Retarded and Advanced components $g^{R/A}$ carry information about the density of states and correlations, while g^K encodes the quasiparticles' dynamics and distribution function. Each of the three components are 4×4 matrices, parametrized by outer products of 2×2 Pauli matrices in spin and particle-hole spaces $\sigma_i \otimes \tau_j$ $(i,j = x,y,z)$.

We use the quasiclassical propagator to compute the density of electronic states (DoS) $N(\boldsymbol{R},\hat{p},\epsilon)$

$$\frac{N(\boldsymbol{R},\hat{p},\epsilon)}{N_F} = -\frac{1}{\pi}\mathrm{Im}\left[\frac{1}{4}\mathrm{Tr}\{\tau_z g^R(\boldsymbol{R},\hat{p},\epsilon)\}\right], \tag{2}$$

and the local heat current $\boldsymbol{j}_h(R)$, and its spectral density $\boldsymbol{j}_h(\boldsymbol{R},\epsilon)$,

$$\begin{aligned}\boldsymbol{j}_h(\boldsymbol{R}) &= 2N_F v_F \int_{-\infty}^{+\infty}\frac{d\epsilon}{4\pi i}\int d\hat{p}\;\epsilon\hat{p}\;\frac{1}{4}\mathrm{Tr}\{g^K(\boldsymbol{R},\hat{p},\epsilon)\}\\ &\equiv \int_{-\infty}^{+\infty} d\epsilon\;\boldsymbol{j}_h(\boldsymbol{R},\epsilon)\,.\end{aligned} \tag{3}$$

Here, N_F is the density of state at the Fermi energy per spin in the normal metallic state, v_F is the Fermi velocity, and $\mathrm{Tr} = \mathrm{Tr}_4$ is the trace operator over spin and Nambu space. $\int d\hat{p}\;\cdots = \langle\ldots\rangle_{\hat{p}} = \int\frac{d\phi_{\hat{p}}}{2\pi}\ldots$ is the normalized Fermi surface integral. We note that to write the heat current as a 4-trace over spin *and* particle-hole space instead of a usual spin-trace over just the upper left component of g^K, we used the symmetry of the Keldysh component $g^K(\boldsymbol{R},\hat{p},\epsilon)^{tr} = \tau_y g^K(\boldsymbol{R},-\hat{p},-\epsilon)\tau_y$ [28].

The quasiclassical Green function $\hat{g}$ is normalized

$$\hat{g}^2(\boldsymbol{R},\hat{p},\epsilon) = -\pi^2\,,\quad \mathrm{Tr}\{g^{R,A}\} = 0\,, \tag{4}$$

and satisfies the Eilenberger equation

$$[\epsilon\hat{\tau}_z - \hat{\sigma},\hat{g}] + iv_F\hat{p}\cdot\boldsymbol{\nabla}\hat{g} = 0\,, \tag{5}$$

where the 8×8 self-energy $\hat{\sigma}(\boldsymbol{R},\hat{p},\epsilon)$ has the same structure in Keldysh space as Eq. (1) and $\hat{\tau}_z = \mathrm{diag}(\tau_z,\tau_z)$. The retarded and advanced components for a singlet superconductor are parametrized as follows $(\mathrm{x} = R,A)$:

$$\sigma^{\mathrm{x}} = \begin{pmatrix} \Sigma^{\mathrm{x}} & \Delta^{\mathrm{x}}(i\sigma_y) \\ (i\sigma_y)\tilde{\Delta}^{\mathrm{x}} & \tilde{\Sigma}^{\mathrm{x}} \end{pmatrix}, \tag{6}$$

and the Keldysh part is

$$\sigma^K = \begin{pmatrix} \Sigma^K & \Delta^K(i\sigma_y) \\ -(i\sigma_y)\tilde{\Delta}^K & -\tilde{\Sigma}^K \end{pmatrix}. \tag{7}$$

The components of these matrices are related to each other through symmetries [28] defined by the $\tilde{}$-operation, which reverses the momentum and energy of complex-conjugated quantities, e.g., $\tilde{\Delta}^{\mathrm{x}}(\boldsymbol{R},\hat{p},\epsilon) = \Delta^{\mathrm{x}}(\boldsymbol{R},-\hat{p},-\epsilon)^*$. The diagonal self-energy terms $\Sigma,\tilde{\Sigma}$ are due to impurity scattering effects. The off-diagonal terms contain the mean-field order parameter and impurity contributions:

$$\Delta^{R/A}(\boldsymbol{R},\hat{p},\epsilon) = \Delta(\boldsymbol{R},\hat{p}) + \Delta^{R/A}_{\mathrm{imp}}(\boldsymbol{R},\epsilon),$$

while the Keldysh mean fields are identically zero, leaving only the impurity contributions

$$\Delta^K(\boldsymbol{R},\epsilon) = \Delta^K_{\mathrm{imp}}(\boldsymbol{R},\epsilon)\,.$$

The mean-field order parameter is computed self-consistently from

$$\Delta(\boldsymbol{R},\hat{p}) = \int_{-\epsilon_c}^{+\epsilon_c}\frac{d\epsilon}{4\pi i}\int d\hat{p}'\;V(\hat{p},\hat{\boldsymbol{p}}')\;f^K(\boldsymbol{R},\hat{p},\epsilon)\,. \tag{8}$$

The pairing interaction is $V(\hat{p},\hat{p}') = V_0\,\mathcal{Y}(\hat{p})\mathcal{Y}^*(\hat{p}')$ and $f^K = \frac{1}{4}\mathrm{Tr}\{\frac{\tau_x+i\tau_y}{2}(-i\sigma_y)g^K\}$ is the upper-right singlet component of the Keldysh Green's function. The momentum space basis functions are $\mathcal{Y}(\hat{p}) = 1$ for s-wave, and $\mathcal{Y}(\hat{p}) = \cos 2(\phi_{\hat{p}} - \alpha)$ for d-wave symmetries. The cutoff energy ϵ_c and the interaction amplitude V_0 are eliminated, in the usual manner, in favor of the clean-case transition temperature T_c.

The impurity self-energy part is self-consistently determined within the $\hat{t}$-matrix approximation. For randomly distributed isotropic scattering centers, the 8×8 $\hat{t}$-matrix equation is $\hat{t} = u\hat{1} + u\langle\hat{g}\rangle_{\hat{p}}\hat{t}$, and the self-energy is defined as $\hat{\sigma}_{\mathrm{imp}} = c_{\mathrm{imp}}\hat{t}$. Using traditional definitions of impurity scattering rate $\Gamma = c_{\mathrm{imp}}/\pi N_F$ and phase shift $\tan\delta = u\pi N_F$ in terms of impurity concentration c_{imp} and amplitude u of the pointlike scattering potential, the 4×4 self-energy matrices are determined from $(\mathrm{x} = R,A)$

$$\begin{aligned}\sigma^{\mathrm{x}}_{\mathrm{imp}}(\boldsymbol{R},\epsilon) &= \Gamma\tan\delta + \tan\delta\left\langle\frac{g^{\mathrm{x}}(\boldsymbol{R},\hat{p},\epsilon)}{\pi}\right\rangle_{\hat{p}}\sigma^{\mathrm{x}}_{\mathrm{imp}}(\boldsymbol{R},\epsilon)\,,\\ \sigma^K_{\mathrm{imp}}(\boldsymbol{R},\epsilon) &= \frac{1}{\Gamma}\sigma^R_{\mathrm{imp}}(\boldsymbol{R},\epsilon)\left\langle\frac{g^K(\boldsymbol{R},\hat{p},\epsilon)}{\pi}\right\rangle_{\hat{p}}\sigma^A_{\mathrm{imp}}(\boldsymbol{R},\epsilon)\,.\end{aligned} \tag{9}$$

Impurity scattering suppresses the amplitude of d-wave order parameter (completely, when $T_c \lesssim \Gamma\sin^2[\delta]$), however, the more important effects come in through the density of states and self-energies. In the following, we will mainly make comparison between the Born ($\delta\to 0$) and unitary ($\delta = \pi/2$) limits. In the absence of inelastic scattering, the self-consistent calculation of impurity σ_{imp} and order parameter Δ that includes nonequilibrium effects, guarantees conservation of energy and charge. In particular, self-consistent calculations of self-energies including corrections due to the heat flow will automatically satisfy $\mathrm{div}\,\boldsymbol{j}_h(\boldsymbol{R},\epsilon) = 0$ - condition of no energy accumulation, see Appendix A.

The solution of the self-consistent system of coupled equations for nonuniform states is most conveniently obtained using Riccati parametrization [29]. The retarded ($-$ sign) and advanced ($+$ sign) Green's functions are given by

$$g^{\mathrm{x}} = \frac{\mp i\pi}{1+\gamma^{\mathrm{x}}\tilde{\gamma}^{\mathrm{x}}}\begin{pmatrix} 1-\gamma^{\mathrm{x}}\tilde{\gamma}^{\mathrm{x}} & 2\gamma^{\mathrm{x}}(i\sigma_y) \\ -2\tilde{\gamma}^{\mathrm{x}}(i\sigma_y) & -(1-\tilde{\gamma}^{\mathrm{x}}\gamma^{\mathrm{x}})\end{pmatrix}, \tag{10}$$

where $\gamma^{\mathrm{x}}(\boldsymbol{R},\hat{p},\epsilon)$ are retarded/advanced scalar coherence functions that are zeros in the bulk normal state. The Keldysh

component takes the form

$$g^K = \frac{-2\pi i}{(1+\gamma^R\tilde{\gamma}^R)(1+\gamma^A\tilde{\gamma}^A)} \times \begin{pmatrix} x^K + \gamma^R\tilde{x}^K\tilde{\gamma}^A & -(\gamma^R\tilde{x}^K - x^K\gamma^A)i\sigma_y \\ -i\sigma_y(\tilde{\gamma}^R x^K - \tilde{x}^K\tilde{\gamma}^A) & \tilde{x}^K + \tilde{\gamma}^R x^K\gamma^A \end{pmatrix}, \tag{11}$$

where $x^K(\boldsymbol{R},\hat{p},\epsilon)$ is the (scalar) distribution function. We explicitly took out the singlet spin dependence of coherence amplitudes, compared with Ref. [29], where the coherence functions are spin matrices. The coherence and distribution amplitudes are related to each other through $\tilde{}$ relation, as well as [29]

$$\begin{aligned} \gamma^A(\boldsymbol{R},\hat{p},\epsilon) &= -\tilde{\gamma}^R(\boldsymbol{R},\hat{p},\epsilon)^*, \\ x^K(\boldsymbol{R},\hat{p},\epsilon) &= x^K(\boldsymbol{R},\hat{p},\epsilon)^*. \end{aligned} \tag{12}$$

The distribution function is not unique, and the usual choice in equilibrium is

$$x_0^K = \Phi_0(\epsilon/T)(1+\gamma^R\tilde{\gamma}^A), \tag{13}$$

where

$$\Phi_0(\epsilon/T) = \tanh(\epsilon/2T) = 1 - 2f(\epsilon/T)$$

and $f(\epsilon/T) = [\exp(\epsilon/T)+1]^{-1}$ is the Fermi distribution at temperature T. Transportlike equations for coherence and distribution functions follow from Eq. (5):

$$\begin{aligned} &iv_F\hat{p}\cdot\nabla\gamma^{\mathrm{x}} + (2\epsilon - \Sigma^{\mathrm{x}} + \tilde{\Sigma}^{\mathrm{x}})\gamma^{\mathrm{x}} + \tilde{\Delta}^{\mathrm{x}}(\gamma^{\mathrm{x}})^2 + \Delta^{\mathrm{x}} = 0, \\ &iv_F\hat{p}\cdot\nabla x^K + (\gamma^R\tilde{\Delta}^R - \Sigma^R + \Delta^A\tilde{\gamma}^A + \Sigma^A)x^K \\ &\quad = \gamma^R\tilde{\Sigma}^K\tilde{\gamma}^A - \Delta^K\tilde{\gamma}^A - \gamma^R\tilde{\Delta}^K - \Sigma^K. \end{aligned} \tag{14}$$

A. Linear response

In the absence of heat current, $\boldsymbol{j}_h = 0$, the system is assumed in global equilibrium at temperature T, with $x^K = x_0^K(\boldsymbol{R},\hat{p},\epsilon)$ given by Eq. (13), and equilibrium coherence functions $\gamma^{\mathrm{x}} = \gamma_0^{\mathrm{x}}(\boldsymbol{R},\hat{p},\epsilon)$ found from

$$iv_F\hat{p}\cdot\nabla\gamma_0^{\mathrm{x}} + \left(2\epsilon - \Sigma_0^{\mathrm{x}} + \tilde{\Sigma}_0^{\mathrm{x}}\right)\gamma_0^{\mathrm{x}} + \tilde{\Delta}_0^{\mathrm{x}}\left(\gamma_0^{\mathrm{x}}\right)^2 + \Delta_0^{\mathrm{x}} = 0. \tag{15}$$

In uniform superconductors, $\nabla\gamma_0^{\mathrm{x}}(\boldsymbol{R},\hat{p},\epsilon) = 0$, and the solution of Eq. (15) for the retarded coherence function is

$$\gamma_u^R(\hat{p},\epsilon) = -\frac{\Delta_u^R}{\bar{\epsilon}^R + i\sqrt{\Delta_u^R\tilde{\Delta}_u^R - (\bar{\epsilon}^R)^2}}, \tag{16}$$

with $\bar{\epsilon} = \epsilon - (\Sigma_u^R - \tilde{\Sigma}_u^R)/2$. In the following, the subscript "u" stands for uniform and subscript "0" will refer to the equilibrium solution.

In the presence of a small heat current $\boldsymbol{j}_h \neq 0$ that is assumed to be time-independent (stationary state), the system is out of equilibrium. In linear response, we expand the coherence and distribution functions around their equilibrium values:

$$\begin{aligned} \gamma^{\mathrm{x}}(\boldsymbol{R},\hat{p},\epsilon) &= \gamma_0^{\mathrm{x}}(\boldsymbol{R},\hat{p},\epsilon) + \gamma_1^{\mathrm{x}}(\boldsymbol{R},\hat{p},\epsilon), \\ x^K(\boldsymbol{R},\hat{p},\epsilon) &= \Phi_0(\epsilon)\left(1+\gamma_0^R\tilde{\gamma}_0^A\right) \\ &\quad + \Phi_0(\epsilon)\left(\gamma_0^R\tilde{\gamma}_1^A + \gamma_0^R\tilde{\gamma}_1^A\right) + x^a. \end{aligned} \tag{17}$$

The deviation of the distribution function from equilibrium, $x^K - x_0^K$, is described by two terms. The first accounts for a change in the density of states through corrections to the retarded and advanced functions; it is weighted by the equilibrium Fermi distribution $\Phi_0(\epsilon)$. The second term, $x^a(\boldsymbol{R},\hat{p},\epsilon)$, is the anomalous, or dynamical distribution function. It determines the dynamical part of the Keldysh Green's function $\hat{g}^a = \hat{g}^K - \hat{g}_0^K - \Phi_0(\hat{g}_1^R - \hat{g}_1^A)$,

$$\hat{g}^a = \frac{-2\pi i}{\left(1+\gamma_0^R\tilde{\gamma}_0^R\right)\left(1+\gamma_0^A\tilde{\gamma}_0^A\right)} \times \begin{pmatrix} x^a + \tilde{x}^a\gamma_0^R\tilde{\gamma}_0^A & \left(x^a\gamma_0^A - \tilde{x}^a\gamma_0^R\right)i\sigma_y \\ -i\sigma_y\left(x^a\tilde{\gamma}_0^R - \tilde{x}^a\tilde{\gamma}_0^A\right) & \tilde{x}^a + x^a\tilde{\gamma}_0^R\gamma_0^A \end{pmatrix}. \tag{18}$$

In linear response, the heat current depends only on the *equilibrium* spectral properties through coherence amplitudes $\gamma_0^{R,A}$, and the dynamical part of distribution function, x^a:

$$\boldsymbol{j}_h = -2N_F v_F \int_{-\infty}^{+\infty} d\epsilon \times \left\langle \epsilon\hat{p}\,\frac{x^a\left(1+\tilde{\gamma}_0^R\gamma_0^A\right) + \tilde{x}^a\left(1+\gamma_0^R\tilde{\gamma}_0^A\right)}{4\left(1+\gamma_0^R\tilde{\gamma}_0^R\right)\left(1+\gamma_0^A\tilde{\gamma}_0^A\right)} \right\rangle_{\hat{p}}. \tag{19}$$

To obtain an equation for x^a, we linearize Eq. (14). We linearize with respect to the global equilibrium at temperature T, where $\Phi_0(\epsilon/2T)$ in Eq. (17) is position-independent. In this case the linearized equation reads [29]

$$iv_F\hat{p}\cdot\nabla x^a + \frac{iv_F}{\ell(\boldsymbol{R},\hat{p},\epsilon)}x^a = \gamma_0^R\tilde{\gamma}_0^A\tilde{\Sigma}^a - \left(\Delta^a\tilde{\gamma}_0^A + \tilde{\Delta}^a\gamma_0^R + \Sigma^a\right), \tag{20}$$

with an equation for the $\tilde{x}^a$ function obtained from this one by employing the definition of $\tilde{}$ operation. In the above equations, we introduced the parameter

$$\ell(\boldsymbol{R},\hat{p},\epsilon) = iv_F/\left(\gamma_0^R\tilde{\Delta}_0^R - \Sigma_0^R + \tilde{\gamma}_0^A\Delta_0^A + \Sigma_0^A\right), \tag{21}$$

which is purely real, as follows from the symmetries of the coherence functions and self-energies and has dimension of length. In the normal metallic phase, $\ell = v_F/2\Gamma\sin^2\delta = v_F\tau_N = \ell_N$ matches with the elastic mean-free path. The dynamical self-energy entering Eq. (20) as the source term is self-consistently computed from x^a and γ_0^{x}:

$$\begin{aligned} \sigma^a(\boldsymbol{R},\epsilon) \equiv \sigma^a_{\mathrm{imp}} &\equiv \begin{pmatrix} \Sigma^a & (i\sigma_y)\Delta^a \\ -(i\sigma_y)\tilde{\Delta}^a & -\tilde{\Sigma}^a \end{pmatrix} \\ &= \frac{1}{\Gamma}\sigma^R_{0,\mathrm{imp}}(\boldsymbol{R},\epsilon)\left\langle\frac{g^a(\boldsymbol{R},\hat{p},\epsilon)}{\pi}\right\rangle_{\hat{p}}\sigma^A_{0,\mathrm{imp}}(\boldsymbol{R},\epsilon). \end{aligned} \tag{22}$$

Note that the linearization scheme in Eq. (17) is very convenient because the calculation of $\boldsymbol{j}_h$ only requires the knowledge of the anomalous x^a, which itself does not depend on spectral corrections γ_1^{x}.

B. Boundary conditions

To solve the transport equation Eq. (20) for the distribution function, one needs to provide suitable boundary conditions for initial values of x^a at the beginning of a trajectory $v_F\hat{p}$, and for final value of $\tilde{x}^a$ at the end of this trajectory. For weak links, as in reference [20], one can assume that the system of interest is connected to large reservoirs in equilibrium at temperatures $T_{1,2}$. Then, for a given quasiparticle trajectory, one can take equilibrium values of the coherence and dynamical amplitudes in those reservoirs as initial values.

Such assumption seems inadequate to compute heat transport in bulk samples. Instead, given a stationary conserved heat flow in the entire sample, we will construct the Riccati amplitudes at $x = \pm L$ in a way that is consistent with Eq. (20), and would give a fixed thermal current

$$\boldsymbol{j}_h(\pm L) = \boldsymbol{j}_h = \boldsymbol{j}_h^{\rm BC} \tag{23}$$

in a uniform superconducting state, away from the inhomogeneous region.

To write such boundary condition, we start by making a trivial observation that the linearization procedure that we followed, can be used to find *equilibrium* functions at slightly different temperature $T + \delta T$. For example, the distribution function can be written as

$$x^K_{eq}(T+\delta T) = [1+\gamma_0^R(T+\delta T)\tilde{\gamma}_0^A(T+\delta T)] \times \Phi_0\left(\frac{\epsilon}{2(T+\delta T)}\right),$$

where we show only the temperature argument explicitly. Decomposition (17) in this case gives the anomalous contribution as

$$x^a_{eq}(T+\delta T) = \left[1+\gamma_0^R(T)\tilde{\gamma}_0^A(T)\right]\frac{\partial\Phi_0}{\partial T}\delta T\,, \tag{24}$$

with $\partial\Phi_0/\partial T = -\epsilon/[2T^2\cosh^2(\epsilon/2T)]$. This x^a_{eq} distribution function, on the other hand, also satisfies Eq. (20) with appropriately determined self-energy through Eq. (22) that can be brought to the form $\sigma^a(T) = (\sigma^R_{0,\rm imp} - \sigma^A_{0,\rm imp})(\partial\Phi_0/\partial T)\delta T$. Far from the region of spatially varying order parameter, the equilibrium functions, $\gamma_0^{R/A}(\hat{p},\epsilon)$ and $x_0^K(\hat{p},\epsilon)$ take their uniform values $\gamma_0^{\rm x} = \gamma_u^{\rm x}$, that determine the scattering length ℓ_u through Eq. (21), and in equilibrium $\nabla x^a_{eq} \propto \nabla T = 0$.

When a stationary thermal current flows, a local temperature gradient builds up and $\delta T(\boldsymbol{R}) = T(\boldsymbol{R}) - T$ is a function of position, see Fig. 2. As a result, Eq. (24) with local $\delta T(\boldsymbol{R})$ is no longer a solution to Eq. (20). However, one can modify x^a_{eq} to include the temperature gradient:

$$x^a_u(\boldsymbol{R},\hat{p},\epsilon) = \left[1+\gamma_u^R(\hat{p},\epsilon)\tilde{\gamma}_u^A(\hat{p},\epsilon)\right]\frac{\partial\Phi_0}{\partial T} \times [\delta T(\boldsymbol{R}) - \ell_u(\hat{p},\epsilon)\hat{p}\cdot\nabla T]\,. \tag{25}$$

This expression with uniform gradient $\nabla T = \text{const}$ satisfies Eq. (20). The ∇T term in Eq. (25) is odd in momentum, and after angular integration in Eq. (22) it does not contribute to self-energy σ^a in even-$\hat{p}$ superconductor. Consequently, only the first term, $\propto \delta T(\boldsymbol{R})$, determines the dynamical self-energy. In entirely uniform superconductor, x^a and $\tilde{x}^a$ would be trivially related and result in local equilibrium

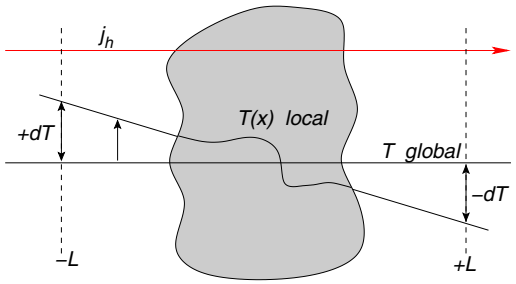

FIG. 2. Local vs global equilibrium picture. The system is driven out of equilibrium by a steady uniform heat current j_h. The local equilibrium picture assumes that when heat flows, a local temperature $T(x)$ can be defined, and its gradient determines the magnitude of j_h. It is typically used in uniform-state problems, and we use it here to define boundary conditions for distribution functions away from the nonuniform (shaded) region of the order parameter. Our main approach, however, is to expand the propagators around some global equilibrium value of the temperature T: $g(x) = g_{\rm eq}(T) + g_c(x)$ where $g_c(x)$ determines current j_h.

self-energy $\sigma^a_u = (\sigma^R_{0,\rm imp} - \sigma^A_{0,\rm imp})(\partial\Phi_0/\partial T)\,\delta T(\boldsymbol{R})$. This is important since after substitution of this expression together with Eq. (25) into Eq. (20) the arbitrary $\delta T(\boldsymbol{R})$ drops out. Nonuniform order parameter means different history for $x^a(\hat{p})$ and $\tilde{x}^a(\hat{p})$ along a trajectory and the self-energy σ^a even in uniform part does not fully recover the local equilibrium dependence on δT.

On the other hand, by similar symmetry arguments, the heat current in the uniform part of the superconductor is independent of δT and is completely determined by the ∇T term of x^a_u. We use it to set the value of the temperature gradient from fixed $\boldsymbol{j}_h^{\rm BC}$. Inserting Eq. (25) into Eq. (19), and using γ-symmetries Eq. (12), we obtain a uniform-state current

$$\boldsymbol{j}_h^{\rm BC} = -\kappa_u\nabla T\,, \quad \kappa_u = \int_{-\infty}^{+\infty} d\epsilon\,\kappa_u(\epsilon)\,, \tag{26}$$

where the thermal conductivity has this Boltzmann-like representation

$$\kappa_u(\epsilon) = \frac{v_F\epsilon^2}{2T^2\cosh^2(\epsilon/2T)}\left\langle\hat{p}_x^2 N(\hat{p},\epsilon)v(\hat{p},\epsilon)\bar{\tau}(\hat{p},\epsilon)\right\rangle_{\hat{p}}\,. \tag{27}$$

Here, $N(\hat{p},\epsilon)$ is the density of states, $\bar{\tau}(\hat{p},\epsilon) = [\ell(\hat{p},\epsilon) + \tilde{\ell}(\hat{p},\epsilon)]/2v_F$ is a scattering time defined using relaxation length (21) [in the unitary or Born limits $\ell(\hat{p},\epsilon) = \tilde{\ell}(\hat{p},\epsilon) \equiv \ell(-\hat{p},-\epsilon)$]. The group velocity for quasiparticles (QPs) with momentum $\hat{p}$ and energy ϵ is given by

$$v(\epsilon,\hat{p}) = v_F\frac{1-\left|\gamma_u^R(\hat{p},\epsilon)\right|^2}{1+\left|\gamma_u^R(\hat{p},\epsilon)\right|^2}\,. \tag{28}$$

From this, the velocity of QPs in superconductor is always smaller than v_F; also in the clean limit one recovers the well-known result $v(\hat{p},\epsilon) = v_F\sqrt{\epsilon^2-\Delta^2(\hat{p})}/|\epsilon|$. Typically, heat transport in uniform superconductors is analyzed as interplay between the density of states $N(\hat{p},\epsilon)$ and effective elastic mean-free path

$$\ell_e \equiv \bar{\tau}(\hat{p},\epsilon)v(\hat{p},\epsilon)\,, \tag{29}$$

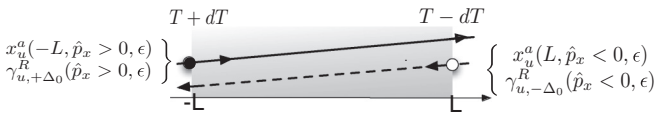

FIG. 3. Numerical integrations of Eqs. (15) and (20), in the shaded region, performed from $x = \mp L$ to $x = \pm L$ for right/left going ($\hat{p}_x \lessgtr 0$) trajectories along $\hat{p}$. We start the numerical integration at the white/black circles with the uniform Riccati amplitude given by Eqs. (30) and (31), see main text. The (half-) temperature bias dT is the unknown that we numerically determine to satisfy Eq. (23).

where the latter plays a more dominant role. This discussion is moved to Appendix B, with the main result presented in Figs. 12 and 11 there.

We are now ready to write the initial values of coherence and distribution functions for numerical integration Eqs. (15) and (20) along quasiclassical trajectories. We start the integration well away from any domain walls, inside the uniform part of superconductor, at $x = \pm L$, Fig. 2. The distance between the initial point on the trajectory and the first domain wall should be much greater than $\ell(\hat{p},\epsilon)$, which might be difficult to satisfy for all energies and momenta, especially in clean superconductor.

The equilibrium coherence functions at $x = \pm L$ arrive from infinity with the uniform bulk values, Fig. 3:

$$\begin{aligned}\gamma_0^R(-L,\hat{p}_x>0,\epsilon) &= \gamma^R_{u,0}(\Delta(x=-\infty,\hat{p}),\hat{p},\epsilon)\,,\\ \gamma_0^R(+L,\hat{p}_x<0,\epsilon) &= \gamma^R_{u,0}(\Delta(x=+\infty,\hat{p}),\hat{p},\epsilon)\,.\end{aligned} \tag{30}$$

We will position the center of domain walls symmetrically around $x = 0$, ensuring equivalent temperature drops dT on the left and right, to accelerate numerical integration. The initial values for the anomalous distribution $x^a(\pm L)$ is given by Eq. (25) with temperature gradient fixed by the heat current in uniform region:

$$\begin{aligned}\nabla T &= -\frac{j_h^{\rm BC}}{\kappa_u}\,\hat{x}\,,\\ x^a(-L,\hat{p}_x>0,\epsilon) &= \left(1+\gamma_u^R\tilde{\gamma}_u^A\right)\frac{\partial\Phi_0}{\partial T}[dT+\ell\,\hat{p}\cdot\nabla T]\,,\\ x^a(L,\hat{p}_x<0,\epsilon) &= \left(1+\gamma_u^R\tilde{\gamma}_u^A\right)\frac{\partial\Phi_0}{\partial T}[-dT+\ell\,\hat{p}\cdot\nabla T]\,.\end{aligned} \tag{31}$$

The unknown temperature drop dT is determined, for a given j_h, through self-consistent calculation of anomalous self-energies $\sigma^a(x,\epsilon)$ at each ϵ. Starting with some guess for $\sigma^a(x,\epsilon)$ we solve Eq. (20) for $x^a(x,\hat{p},\epsilon)$ with boundary conditions (31). From distribution function, we find $g^a(x,\hat{p},\epsilon)$, Eq. (18), and then obtain new values for $\sigma^a(x,\epsilon)$, Eq. (22). This process is repeated until self-energy has converged. The linearity of all equations assures that all the parameters are linear combinations of dT and ∇T terms:

$$\begin{aligned}x^a(x,\hat{p},\epsilon) &= x_1^a(x,\hat{p},\epsilon)dT + x_2^a(x,\hat{p},\epsilon)\nabla T\,,\\ g^a(x,\hat{p},\epsilon) &= g_1^a(x,\hat{p},\epsilon)dT + g_2^a(x,\hat{p},\epsilon)\nabla T\,,\\ \sigma^a(x,\epsilon) &= \sigma_1^a(x,\epsilon)dT + \sigma_2^a(x,\epsilon)\nabla T\,,\end{aligned} \tag{32}$$

and similarly the current, $j_h(x) = \kappa_1 dT + \kappa_2\nabla T = \text{const} = \kappa_u\nabla T$, that is equal to the input current at the boundary. After self-consistent determination of the coefficients $\kappa_{1,2}$ through the above procedure, we determine the temperature drop

$$dT = \frac{\kappa_u - \kappa_2}{\kappa_1}\nabla T\,.$$

In the uniform case, one has $dT = Lj_h^{BC}/\kappa_u$.

Here we also want to note that the presence of topological domain walls in the order parameter is reflected in features of the heat current arbitrarily far from the nonuniform region, and is indirectly encoded in the choice (31) for x^a at the integration boundaries. For example, in a uniform superconductor, the spectral current is given by $\kappa_u(\epsilon)|\nabla T|$, whereas in nonuniform superconductor we have $j_h(\epsilon) \neq \kappa_u(\epsilon)|\nabla T|$, which is obvious if we are right at the domain wall, and thus everywhere else due to the conservation of the spectral current, as shown in Appendix A. To recover the heat current spectrum of the uniform state far from the nonuniform region, one requires presence of nonelastic collisions that are not included in the theory. By contrast, the local equilibrium picture includes the nonelastic collisions implicitly in the definition of the local temperature $T(x)$ in Fermi distribution.

IV. HEAT FLOW ACROSS DOMAIN WALLS

We now apply the developed formalism to nonuniform d-wave superconductor, and investigate heat transport across an array of $N_{\rm DW}$ domains walls equally spaced with a period $X_{\rm FFLO}$ along the $\hat{x}$ axis. Each domain wall has a width of several coherence lengths that we define as

$$\xi = \frac{\hbar v_F}{2\pi k_B T_c}$$

(T_c is the transition temperature of clean supercnductor). The uniform heat current flows from left to right $\boldsymbol{j}_h = j_h\hat{x}$, and we consider translationally invariant system along the $\hat{y}$ direction, so that all functions depend only on x coordinate.

For convenience, we now set a unit gradient at the boundaries $\nabla T = -\hat{x}$ in Eq. (31), giving $j_h = \kappa_u \times 1$. Due to the factor $|\epsilon\,\partial_T\Phi_0| = \epsilon^2/[2T^2\cosh^2(\epsilon/2T)]$, the heat current is mainly determined by quasiparticles with energies in the window $[T,5T]$. We introduce $\epsilon_T = 2.5\,T$ as a characteristic quasiparticle energy at a given temperature T.

A. Single domain wall

We first look at the heat transport across a single domain wall (DW) centered at $x = 0$ ($N_{\rm DW} = 1$). The domain wall is enforced through the boundary condition $\Delta_0(\pm L) = \pm\Delta_u$. It is self-consistently computed together with the local impurity self-energy $\sigma_{\rm imp}(x,\epsilon)$ via Eqs. (8) and (9).

With the domain wall centered at $x = 0$, we use symmetry $\Delta(-x) = -\Delta(x)$ to speed up numerical calculations through relations:

$$\begin{aligned}\gamma_0^R(x,\hat{p},\epsilon) &= -\gamma_0^R(-x,-\hat{p},\epsilon),\\ \gamma_0^R(x,\hat{p},\epsilon) &= -\tilde{\gamma}_0^R(x,-\hat{p},\epsilon),\end{aligned} \tag{33}$$

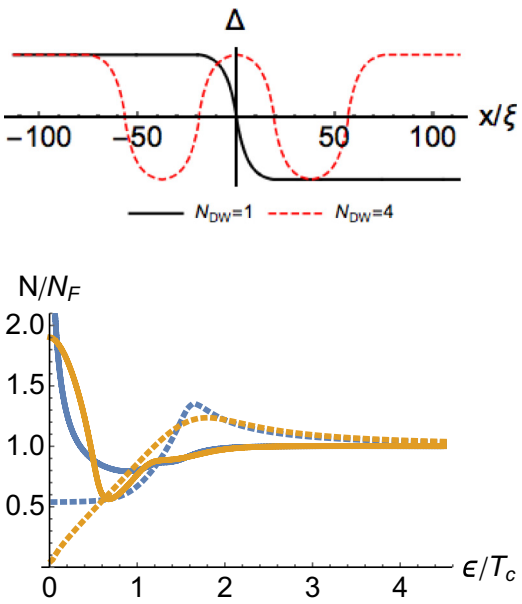

FIG. 4. (Top) Self-consistent OP profile $\Delta(x)$ for a single DW (solid line). This solution is used to construct a non-self-consistent profile with $N_{\rm DW}$, case of 4 DWs with separation $X_{\rm FFLO} \approx 20\xi$ is shown by the dashed line. (Bottom) Local density of states (DoS) in Born (orange) and unitary (blue) limits for $\ell_{\rm N} = \pi\xi/0.3$. At the domain (solid lines), the peak at zero energy indicates the Andreev bound states (ABS).

and similar ones for self-energies:

$$\begin{aligned} \sigma^R(x,\hat{p},\epsilon) &= \tau_z \sigma^R(-x,\hat{p},\epsilon)\tau_z, \\ \sigma^R(x,\hat{p},\epsilon) &= [\sigma^R(x,\hat{p},\epsilon)]^{tr}, \\ \sigma^a(x,\epsilon) &= -\tau_z \sigma^a(-x,\epsilon)\tau_z\,. \end{aligned} \tag{34}$$

Technically we proceed as follows. First, we obtain the order parameter profile $\Delta_0(x)$, shown in Fig. 4(a), using the Matsubara technique. With the known mean-field profile, we integrate Eq. (15) for real energies to determine the equilibrium values of $\gamma_0^R(x,\hat{p},\epsilon)$ and impurity $\sigma_{0,\rm imp}^{R/A}(x,\epsilon)$. They are then used as input parameters in Eq. (20) for the anomalous amplitude x^a. The last step is the self-consistent calculation of the temperature drop dT together with anomalous self-energy σ^a.

We compare the temperature drop dT with the drop $dT_u = (j_h/\kappa_u)L = |\nabla T|_u L$ that would appear if the superconductor was uniform. Then $dT > dT_u$ corresponds to a suppression of ability to transport heat across domain walls, while $dT - dT_u < 0$ represents an enhancement of heat conductivity. The numerical results for transport across the domain wall are presented in Fig. 5, where we plot the temperature drop across a domain wall for a given heat current, relative to the uniform configuration. We define the parameter dL' with dimension of length

$$dL' = \frac{dT - dT_u}{j_h/\kappa_u}\,,$$

which can be interpreted as effective "thermal length" of the domain wall, in units of coherence length ξ.

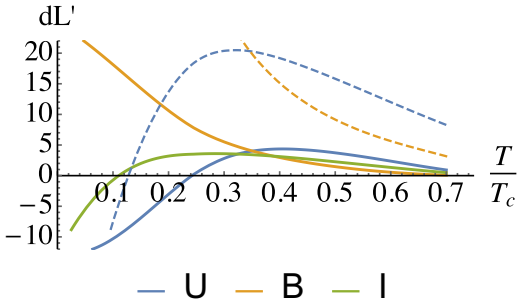

FIG. 5. Effective change in thermal length dL' (in units of ξ) across a single domain wall relative to the uniform case, as function of temperature. Numerical system size is $2L = 16\pi\xi$. Different colors correspond to unitary limit (U, blue), Born (B, orange), and intermediate phase shift $\delta = \pi/4$ (I, green). Solid lines are for scattering rate $2\Gamma \sin^2\delta = 1/\tau_N = 0.6T_c$, dashed lines are for a cleaner case $1/\tau_N = 0.2T_c$. In the unitary limit, dL' is nonmonotonous, and at low temperature $T < W_{\rm imp}$, the heat conductance through a domain wall is larger than in uniform case.

At high temperatures, the behavior of the thermal transport is the same for all impurities, with a loss of effectiveness in energy transport. At low temperatures, however, the behavior is remarkably different in Born and unitary limits. For weak impurity scattering potential, the domain wall presents a barrier for heat transport resulting in a larger temperature drop required to maintain current j_h. The strong scatterers have the opposite effect—the heat current flows through a domain wall more efficiently than in the uniform case. The origin of such peculiar behavior is in the interplay between two effects of the Andreev bound states at the domain wall: the change of spectrum and the hybridization of the bound states with the impurity band states.

The spectral effect is a result of Andreev bound states "stealing" spectral weight from continuum quasiparticles states above the energy gap. In bulk, the only available quasiparticles with $\epsilon > |\Delta(\hat{p})|$ participate in the energy transport. As these quasiparticles enter the domain wall region with fewer available states, they experience Andreev reflection that leads to suppression of the heat conductivity. This effect can be quantified by looking at a clean superconductor. In this case, the equation for the distribution function (20) has no impurity-generated right-hand-side, and the relaxation length (mean-free path) $1/\ell_\Delta = 2\,{\rm Im}[\gamma^R\tilde{\Delta}]/v_F$ is determined purely by the density-of-states effects. Details of this analysis are presented in Appendix C. Effects of the spectral weight reduction and Andreev reflection processes appear in the heat current kernel $K(\epsilon,\hat{p}) = j_h(\hat{p},\epsilon)/(\epsilon\,\partial_T\Phi_0)$, shown in Fig. 6, at energies $\epsilon \sim \Delta$ and play the most important role at higher temperatures.

At very low temperatures $T \ll T_c$, the interaction of low-energy bound states with impurities comes out to the front stage, while we find that ℓ_Δ is only slightly modified by impurities. The impurity scattering effects appear in Eq. (20) through anomalous self-energy and local scattering length $1/\ell_{\rm imp} = 2\,{\rm Im}[\gamma_0^R\tilde{\Delta}_{\rm imp}^R - \Sigma^R]/v_F$. This length is positive and finite, depends on directions very weakly and can be approximated by $\ell_{\rm imp}(x,\epsilon) \approx \langle \ell_{\rm imp}(x,\hat{p},\epsilon)\rangle_{\hat{p}}$. The impurity scattering creates a

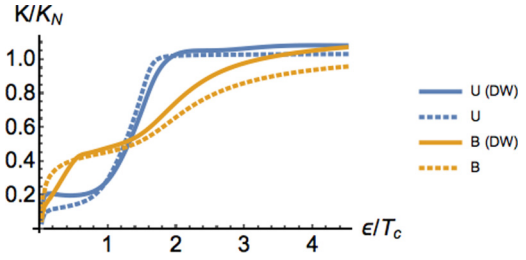

FIG. 6. Energy dependence of the heat current kernel at $T = 0.3T_c$ for transport across a domain wall (solid lines) and the uniform superconductor (dashed lines) for $\ell_N = \pi\xi/0.3$. In Born or clean limit (orange lines), the ability to transport heat at low energy is suppressed by the presence of a domain: at low energy $K_{DW}(\epsilon) < K_u(\epsilon)$. By contrast, in unitary limit (blue lines), the coupling between impurity band and Andreev bound states enhances energy transport: at low energy $K_{DW}(\epsilon) > K_u(\epsilon)$.

band of mid-gap states, which hybridize with Andreev bound states. Such hybridization depends strongly on the strength of the impurities and may lead to a significant "renormalization" of scattering features in the vicinity of the domain wall, as shown in Fig. 7. In the unitary limit, Andreev states' interaction with impurity band leads to suppression of scattering and long lifetime of close-to-zero-energy quasiparticles. This results in an effective "wormhole" across the domain wall region for these quasiparticles, and an enhancement of heat conductivity at low temperature, see Fig. 6. In the Born scattering limit, on the other hand, the impurity band is weak, and its presence cannot compensate Andreev reflections. In this case, for all temperatures, the heat transport is suppressed across the domain wall.

B. Multiple domain walls

To model the periodic structures of FFLO states, we investigate transport across a set of domain walls. Since the main effects come from the density of states and scattering, we omit the self-consistent calculation of the order parameter and simply "build" a lattice of N_{DW} equally spaced domains with an arbitrary period X_{FFLO}, taking the single domain profile

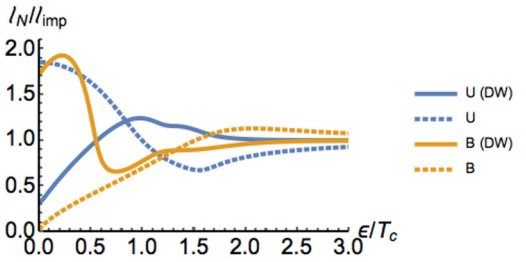

FIG. 7. Inverse local impurity scattering length $\ell_N/\ell_{imp}(x,\hat{p},\epsilon) \approx \ell_N/\ell_{imp}(\epsilon,x)$ (weakly dependent on momentum directions), as a function of energy, for $\ell_N = \pi\xi/0.3$. In Born limit (orange), the mean-free path is large in the bulk (dashed lines) and becomes small at the domain wall (solid lines). For unitary scattering (blue), on the right, this behavior is reversed: the zero-energy peak in the DOS results in suppression of scattering rate at the domain wall and longer mean-free path.

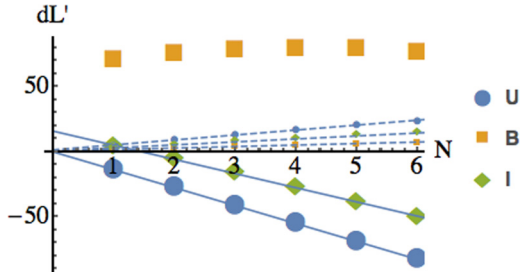

FIG. 8. Effective thermal length dL' (normalized by ξ) across N_{DW} domain walls, for low temperature $T/T_c = 0.05$ (large symbols, solid lines) and intermediate temperature $T/T_c = 0.5$ (small symbols, dashed lines). The scattering rate $1/\tau_N = 0.3T_c$ is used for various impurity strengths: Born (B), unitary (U), and intermediate $\delta = \pi/4$ (I). This is an "independent domain walls" regime where the heat conductivity contributions from each domain add up, as is clear from linear dependency $c_1 N_{DW} + c_2$ shown by lines. At low temperature, the unitary and intermediate strength disorder has a negative slope consistent with the single-domain result in Fig. 5, coming from low-energy states' transport. At intermediate temperature we have a suppression of heat flow due to independent Andreev reflection processes, with positive slope and linear increase in the thermal length dL' with N_{DW}. In the Born limit at low temperature, the dependence is more complicated due to the large extent of bound states and a more intricate impurity band energy dependence for $T \sim W_{imp}$.

as a unit cell, as shown in Fig. 4 for $N_{DW} = 4$. We place the domains symmetrically around $x = 0$ and use this symmetry to reduce computation time.

There are several effects that influence the transport across multiple domain walls. First one is the trivial (incoherent) accumulation of effects from all domains that are independent in this case. This happens when the mean-free path, Eq. (29), is shorter than the spacing X_{FFLO} between domain walls, and the spatial extent of the bound states also exceeds this length, $X_{ABS}[\hat{p}] \approx v_F/\sqrt{\Delta^2(\hat{p}) + W_{imp}^2} \gg X_{FFLO}$, where W_{imp} is the impurity bandwidth. Independent domain walls lead to a linear dependence of the heat conductivity on the number of domain walls N_{DW}, based on the temperature regime and single-domain result as in Fig. 5. Such behavior is expected for reasonably dirty superconductors. Full numerical results for domain wall spacing $X_{FFLO} \approx 18\,\xi$ are shown in Fig. 8 and in the independent-domain regime are fitted with straight lines.

When the superconductor is in the clean limit, and the domain walls are tightly spaced with $X_{FFLO} < X_{ABS}$, the bound states belonging to neighboring domains can overlap, hybridize, and build up a conduction band (hybrid transport). This is expected in FFLO phase when the order parameter is small and harmoniclike, with periods $\sim 5 - 10\xi$ rather than a combination of fully formed domain walls, or when the transport is dominated by the nodal quasiparticles since ABS states can extend far beyond the DW region, especially in the Born limit with a tiny W_{imp}.

If the spacing between the domain walls is somewhat longer, then the hybridization of bound states from different domains depends on their quasiclassical trajectory. In the antinodal direction, the ABS spatial extent is smaller than

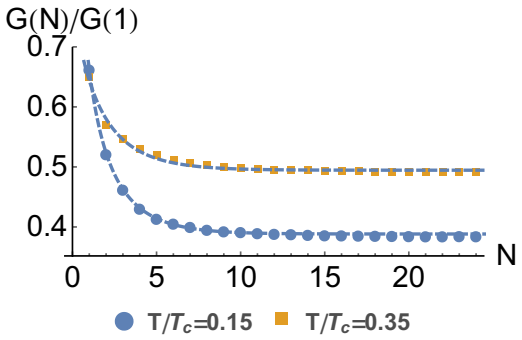

FIG. 9. Effect on thermal conductance of Andreev reflections from a set of $N_{\rm DW}$ domain walls (clean limit). Heat transport through more than ten consecutive domains is dominated by extended bound states along nodal directions on the Fermi surface. Phase space of those states and their contribution to the heat transport grow with temperature. The fitting line through numerical points is explained in the text.

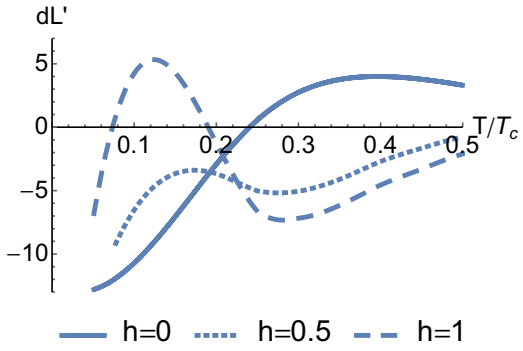

FIG. 10. Effect of the Zeeman field splitting $h = \mu H/T_c$ on thermal transport across a single domain wall. Unitary limit with scattering rate $1/\tau_N = 0.3\,T_c$. The bound states, shifted by $h = 0.5$ contribute to a reduction of the thermal length, dL', in a wide range of temperatures. When the Zeeman shift is very large $h = 1$, the contributions from bound and continuum states mix up leading to a very nonmonotonic temperature dependence.

$X_{\rm FFLO}$ and ABS are spatially separated. Each domain is the center of an Andreev reflection process. Consecutive reflections add up and yield a power law reduction of the transmission of antinodal quasiparticles. By contrast, in the nodal direction, the ABS extent is large. ABS at consecutive domains overlap and the transmission is rather insensitive to the number of domains. Together, they result in $N_{\rm DW}$ dependence seen in Fig. 9. The heat conductance can be roughly fitted by a sum of nodal and antinodal contributions: $g_{\rm n} + g_{\rm an} t^{N_{\rm DW}}$, where the conductance contribution from nodal quasiparticles $g_{\rm n.}$ grows with temperature, and the transmission coefficient t is only weakly temperature-independent.

C. Zeeman field

In this section we present the effects of a Zeeman field on heat transport across the nonuniform state, since the FFLO state is a result of competition between magnetization and condensation energies. Again, the main effect, we assume, is coming from the modification of the density of quasiparticle states that are shifted in energy by $\pm\mu H$ for up/down spins. We neglect the order parameter suppression due to magnetic field, which is relatively small at low temperature [25]. Then the spin-up and spin-down QPs are independent, and their contributions to thermal transport add up.

The dependence on spin enters Eqs. (19), (20), and boundary conditions (25) and (31) through energy shift in coherence functions $\gamma_0^{\rm R/A}(\epsilon \pm \mu H)$. The quasiparticle distribution function prefactor $\epsilon\partial_T\Phi_0(\epsilon,T)$ is not changed. We can use it to write the heat current as some spin-dependent kernel times the distribution function:

$$j_h = \sum_{s=\pm1} \int d\epsilon\, K_s(\epsilon)\, \epsilon\partial_T\Phi_0(\epsilon,T)\,. \tag{35}$$

We then can re-use the zero-field results to compute the thermal current including the Zeeman splitting. In the Zeeman field, the spin-dependent kernel is simply the spin-independent kernel shifted energy: $K_s(\epsilon) = K(\epsilon - s\mu H)$. We then can transfer the dependence on spins into the distribution function, without recalculating the kernel:

$$j_h^H = \frac{1}{2}\sum_{\pm} \int d\epsilon\, j_h^0(\epsilon)\left[\frac{(\epsilon \pm \mu H)\partial_T\Phi_0(\epsilon \pm \mu H,T)}{\epsilon\partial_T\Phi_0(\epsilon,T)}\right], \tag{36}$$

where $j_h^0(\epsilon)$ is the spectral heat current in the absence of Zeeman field. As a reminder, Fig. 6 highlights the effect of impurity on the kernel of heat current in absence of Zeeman field.

The effect of the Zeeman splitting of the states on thermal conductivity across a single domain wall is shown in Fig. 10 for strong impurities. The bound states contribute most to the low-energy heat current and lead to an increase in conductivity at low temperatures, $T \lesssim \Delta\epsilon_{BS}/2.5$. From the $h = 0$ curve, the half-width of the bound states can be estimated as $\Delta\epsilon_{BS} \sim 0.4T_c$. When the Zeeman field shifts the bound states by $h = \mu H/T_c = 0.5$, they dominate the heat transport in a wide range of temperatures leading to negative $dT - dT_u$. For even higher fields $h = 1$, close to the critical field, the contributions of bound states with one spin projection mix with the continuum contribution with the other spin projection, leading to a nonmonotonic temperature dependence of the heat conductivity.

V. CONCLUSIONS

In this paper, we have developed a theoretical framework to investigate thermal transport in nonuniform superconductors. Our approach is based on a fully self-consistent nonequilibrium quasiclassical Eilenberger-Keldysh technique that takes into account, on the same footing, the combined effects of impurity scattering, spatial variations of the order parameter and density of states, and the presence of Andreev bound states in strongly inhomogeneous environments.

We applied this theory to compute the thermal current across the periodic modulations of the order parameter, and domain walls, in a superconductor with d-wave pairing. Here we outline the key effects that govern transport in such systems

compared with the uniform superconductors. First, Andreev bound states "trap" quasiparticles and cause a depletion of the continuum ($\epsilon > \Delta$) states near the domain wall, leading to Andreev reflection processes with particle-hole conversions. This results in a reduction of heat transport across the domain wall, and this mechanism is dominant at intermediate temperatures and in clean superconductors. Another effect becomes relevant at low temperatures when disorder is present. Then the bound states at the domain wall interact with the low-energy impurity band. The coupling of the impurity band to localized Andreev states strongly depends on the type of impurity scattering. In the Born limit, this coupling increases the scattering rate, while in the unitary limit the scattering of low-energy quasiparticles is suppressed. These states have longer mean-free path in the domain wall region resulting in an effective "wormhole" through the domain wall. At low temperature, below the width of the impurity band, transport is dominated by these states and with unitary impurities, the heat conductivity across the domain wall is higher than the conductivity in the uniform state. This results in a very distinct nonmonotonic feature of heat conductivity as a function of temperature, as one crosses from high- into low-energy regime. In a Zeeman field, the difference between thermal transport in uniform and nonuniform phases is softened, but due to the opposite shifts of the up/down spin states, one can observe additional features in the T dependence of the heat conductivity, and a nonmonotonic T dependence appears even in the Born limit. A grid of multiple domain walls generally amplifies the transport properties of a single domain, but in the clean limit one has to consider multiple-wall Andreev backscattering processes.

These results show that thermal transport can be a useful probe to detect and study nonuniform states, such as the Fulde-Ferrell-Larkin-Ovchinnikov phase, which so far has been only identified using NMR technique [27]. The approach that we developed will pave the way for future theoretical studies of heat transport near surfaces of superconductors with nontrivial surface states, in vortex lattices including vortex core states, or for complete analysis of FFLO-type order parameter periodic structures.

ACKNOWLEDGMENTS

This work has been done with NSF support through Grant DMR-0954342.

APPENDIX A: UNIFORMITY OF CURRENTS

In the absence of inelastic scattering processes, the self-consistent solution of the Elenberger transport equation (5) together with the impurity self-energies (9) guarantees uniform heat flow, and nonaccumulation of heat, $\nabla \cdot \boldsymbol{j}_h = -\partial_t Q = 0$, even in the presence of a spatially varying order parameter. The heat current is given by Eq. (3), which we repeat here:

$$\boldsymbol{j}_h(\boldsymbol{R}) = 2N_F v_F \int_{-\infty}^{+\infty} \frac{d\epsilon}{4\pi i} \int d\hat{p}\ [\epsilon\ \hat{p}]\ \frac{1}{4}\mathrm{Tr}\{g^K(\boldsymbol{R},\hat{p},\epsilon)\}\,. \tag{A1}$$

With only energy-conserving impurity collisions, all ϵ are independent, and we can consider the divergence of the heat current kernel for single energy, $\nabla \cdot \boldsymbol{j}_h(\boldsymbol{R},\epsilon) \propto \langle \hat{p} \cdot \mathrm{Tr}\nabla g^K \rangle_{\hat{p}}$. Using the equation for the Keldysh component of Eq. (5),

$$\begin{aligned} i v_F \hat{p}\nabla g^K &= g^K(\epsilon\tau_z - \sigma^A) - (\epsilon\tau_z - \sigma^R)g^K \\ &\quad + \sigma^K g^A - g^R\sigma^K, \end{aligned} \tag{A2}$$

we can split off the mean-field self-energy $\Delta(\boldsymbol{R},\hat{p})$, common for both retarded and advanced functions and zero for the Keldysh component, from the impurity self-energy. This allows us to write

$$\begin{aligned} \langle \hat{p}\,\mathrm{Tr}\nabla \cdot g^K\rangle_{\hat{p}} &\propto -\langle \mathrm{Tr}\{[\epsilon\tau_z - \Delta, g^K]\}\rangle_{\hat{p}} + \mathrm{Tr}\big\{\sigma^R_{\mathrm{imp}}\langle g^K\rangle_{\hat{p}} \\ &\quad - \langle g^K\rangle_{\hat{p}}\sigma^A_{\mathrm{imp}} + \sigma^K_{\mathrm{imp}}\langle g^A\rangle_{\hat{p}} - \langle g^R\rangle_{\hat{p}}\sigma^K_{\mathrm{imp}}\big\} \\ &= -0 + 0, \end{aligned} \tag{A3}$$

where the first term is zero due to the traceless property of a commutator and the second zero follows from the self-consistent relations between impurity self-energies and the Fermi-surface averaged propagators, Eq. (9).

Note that the order parameter self-consistency was not used in the above argument. It is, however, needed to conserve the charge/particle number. The formula for the particle current, written in terms of 4-trace, acquires an extra τ_z matrix (and absence of ϵ factor):

$$\boldsymbol{j}_e(\boldsymbol{R}) = 2N_F v_F \int_{-\infty}^{+\infty} \frac{d\epsilon}{4\pi i} \int d\hat{p}\ \hat{p}\ \frac{1}{4}\mathrm{Tr}\{\tau_z g^K(\boldsymbol{R},\hat{p},\epsilon)\}\,. \tag{A4}$$

Following the same line of arguments as for the heat current above, we notice that the impurity self-energy part vanishes due to same self-consistency as before but the commutator term with the mean-field order parameter is

$$\int d\epsilon \langle \mathrm{Tr}\ \{\tau_z[\epsilon\tau_z - \Delta\ , g^K]\}\rangle_{\hat{p}} = 2\int d\epsilon \langle \mathrm{Tr}\ \{\Delta\tau_z g^K\}\rangle_{\hat{p}}, \tag{A5}$$

which vanishes if one uses the self-consistency on $\Delta(\boldsymbol{R},\hat{p})$, Eq. (8), ensuring nonaccumulation of charge.

APPENDIX B: RELATIVE IMPORTANCE OF DENSITY OF STATES AND MEAN-FREE PATH.

To relate our results and treatment to previous work, in this appendix, we present results for a uniform d-wave superconductor. The heat transport in a typical Boltzmann picture depends on a product of the density of states $N(\hat{p},\epsilon)$ and effective elastic mean-free path,

$$\ell_e \equiv \bar{\tau}(\hat{p},\epsilon)v(\hat{p},\epsilon)\,. \tag{B1}$$

The low-energy spectrum of a d-wave superconductor is strongly modified by the scattering of quasiparticles on impurities due to the anisotropy of the order parameter structure. Scattering on impurities results in the formation of midgap states [30]. These impurity-bound states are extended in space and form a conduction "impurity" band with energy width W_{imp} [2,31]. This bandwidth is tiny in the Born limit, $W^B_{\mathrm{imp}} \approx 4\Delta_0 \exp(-\frac{\pi\Delta_0}{\Gamma})$, but can be large in the unitary limit where $W^U_{\mathrm{imp}} \approx \sqrt{\pi\Delta_0\Gamma/2}$.

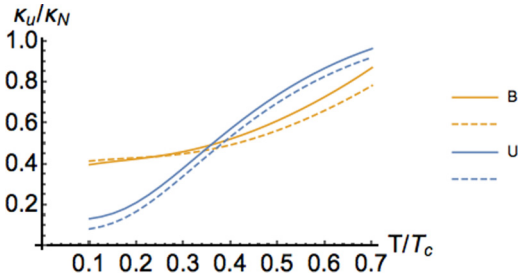

FIG. 11. Uniform thermal conductivity as a function of temperature. At low temperature, $T \lesssim 0.3T_c$ ($\epsilon \lesssim 0.6T_c$), the thermal conductivity in Born limit (green) is higher than that in the Unitary limit (blue), indicating that it is dominated by the large mean-free path of quasiparticles. Solid and dashed lines correspond to mean-free paths $\ell_N = \pi\xi/0.3$ and $\ell_N = \pi\xi/0.2$, respectively.

The mean-free path reflects the effectiveness of the scattering of quasiparticles by impurities. It depends on the concentration Γ and strength δ of impurities, as well as on the available phase space for scattering, given by the properties of the order parameter Δ. At low energy $\epsilon < W^B_{\rm imp} < \Delta$, in the Born limit, impurity scattering is ineffective, $v_F/2\,{\rm Im}[\Sigma^R_{\rm imp}] > \ell_N = v_F\tau_N = v_F/(2\Gamma\sin^2\delta)$, and it allows quasiparticles to travel long distance between scatterings producing large heat transport. By contrast, in the unitary limit, scattering is enhanced $v_F/(2\,{\rm Im}[\Sigma^R_{\rm imp}]) < \ell_N$, i.e., low-energy QPs bind to impurities forming a wide impurity band.

Numerically, we find that thermal transport properties are mainly influenced by the behavior of scattering length $\ell_e(\hat{p},\epsilon)$ rather than that of density of states. In Fig. 11, we plot the temperature dependence of $\kappa_u(T)$, which we analyze using data from Fig. 12. At low-to-intermediate temperature $0.05 < T/T_c < 0.3$, corresponding to energies $W_{\rm imp} \lesssim \epsilon < 0.6T_c$ the DoS in Born limit is small $N^B(\epsilon) < N^U(\epsilon)$, while $\ell^B_e \gg \ell^U_e$, producing $\kappa^B_u(T) > \kappa^U_u(T)$. At higher energy and temperature $0.4 < T/T_c, \epsilon > 0.8T_c$, the result is reversed $\kappa^B_u(T) < \kappa^U_u(T)$, again in agreement with the increase of $\ell^U_e > \ell^B_e$ while having about the same values for the DoS in this energy interval. In the very low-temperature limit, $T \ll W_{\rm imp}$, DoS and scattering effects exactly cancel each other, producing the universal limit for heat conductivity, where it does not depend on the disorder properties [2,32,33].

APPENDIX C: HEAT CONDUCTIVITY OF A CLEAN CONSTRICTION

In this appendix, we evaluate heat transport properties of a spin-singlet superconducting constriction without impurities and discuss the role of Andreev reflection processes. The constriction can be thought of as a narrow bridge connecting two large reservoirs that are assumed to be in equilibrium at temperature $T \pm dT$ ($dT \ll T, T_c$). We define the conductance of the clean constriction as $G = I_h/(2dT)$. The global phases of the superconducting order parameter in the reservoirs $\Delta(\hat{p})\exp(i\varphi_{L,R})$ is set to $\varphi_{L,R} = 0,\pi$. The constriction is assumed to be long and narrow, so we neglect the edge effects. In linear response, the energy transport is governed by Eqs. (15) and (20), with $\sigma_{\rm imp} = 0$. At boundaries, $\gamma(\pm L, \hat{p}_x \lessgtr 0,\epsilon)$ is given by Eq. (30) and we take

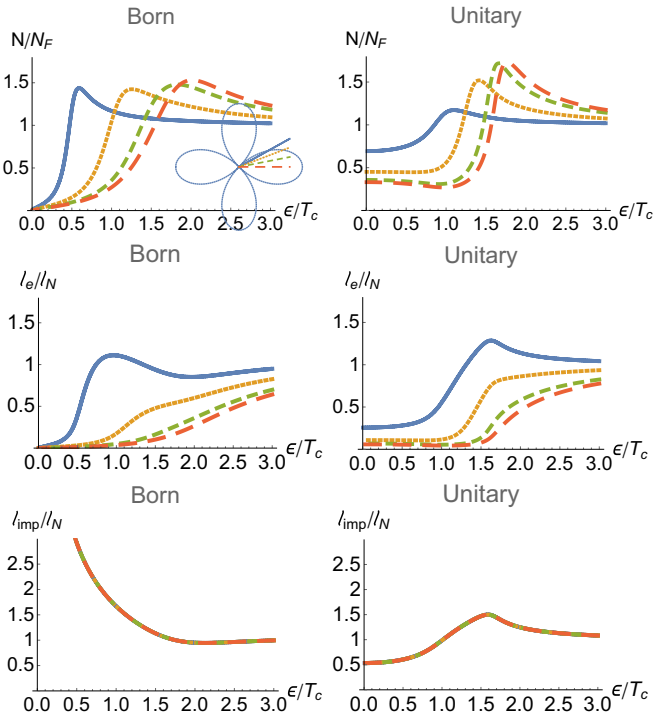

FIG. 12. Spectral and transport properties of a uniform d-wave superconductor. Angle-resolved DoS, $N(\hat{p},\epsilon)/N_F$ (top row), mean-free path $\ell_e(\hat{p},\epsilon)/\ell_N$ (middle row), and impurity scattering length $\ell_{\rm imp}(\epsilon)/\ell_N$ (bottom row) are plotted in Born and unitary limits, for the normal state mean-free path $\ell_N \approx 10\,\xi$, where $\ell_{\rm imp} = v_F/2{\rm Im}[\Sigma_{\rm imp}]$. Different curves represent different momentum directions spanning the d-wave clover from a node to antinode (solid blue to red dashed lines), as shown in inset. In unitary limit, the low-energy impurity band in DoS is large, and the mean-free path is reduced by enhanced impurity scattering. By contrast, in the Born limit, the impurity band is exponentially small and the mean-free path of nodal quasiparticles is longer.

$$x^a_{R/L} = x^a(\pm L, \hat{p}_x \lessgtr 0,\epsilon) = \partial_T\Phi_0(\mp dT)\big(1 + \gamma^R_u\tilde{\gamma}^A_u\big), \tag{C1}$$

which conveniently describes junctions between reservoirs that have negligible heat currents inside. This is different from the boundary condition (31) that was aimed at describing a continuous flow of heat.

The order parameter $\Delta(x)$ and $\gamma_0(x,\hat{p},\epsilon)$ are self-consistently determined throughout the constriction. From equilibrium $\gamma_0(x,\hat{p},\epsilon)$, using Eq. (15), one can find analytic solution for the distribution function along the constriction:

$$\begin{aligned} x^a(x,\hat{p}_x > 0,\epsilon) &= t(x,\hat{p},\epsilon)\,x^a_L, \\ x^a(x,\hat{p}_x < 0,\epsilon) &= t(x,\hat{p},\epsilon)\,x^a_R, \end{aligned} \tag{C2}$$

where

$$t(x,\hat{p},\epsilon) = \frac{1 - \left|\gamma^R_0(x,\hat{p},\epsilon)\right|^2}{1 - \left|\gamma^R_u(\hat{p},\epsilon)\right|^2}, \tag{C3}$$

plays the role of a transmission coefficient ($|t| < 1$). In a uniform superconductor, energy is perfectly transmitted $|t(\epsilon,\hat{p})| = 1$. However, with a domain wall, one has $|t| \leqslant 1$,

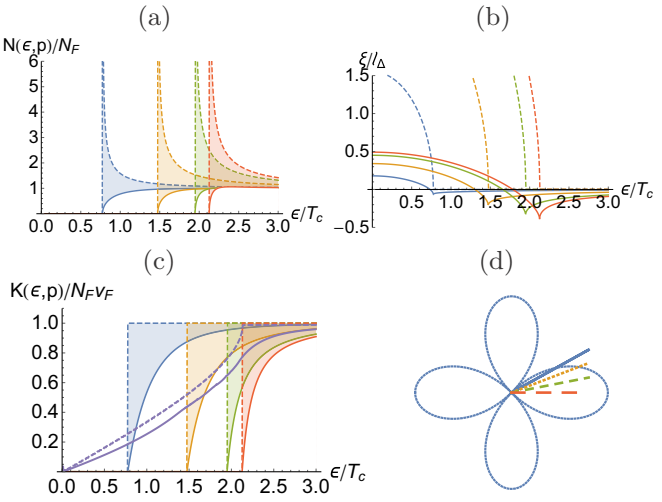

FIG. 13. Thermal transport properties of a clean superconductor across a single domain wall (solid lines) compared against a uniform superconductor (dashed lines). (a) Local DoS for the momenta directions shown in (d) at the domain wall $N(\hat{p},\epsilon,x)$ with part of the spectral weight (shaded area) moved from continuum states into zero-energy bound states, which form a very sharp peak not resolved on this scale. (b) The Andreev reflection length scale $\ell_\Delta(\epsilon,\hat{p},x)$. In a uniform superconductor, it is infinite for above-gap energies $1/\ell_\Delta(|\epsilon| > |\Delta(\hat{p})|) = 0$, while at the domain wall it is finite for all energies and even changes sign. (c) Kernel of the heat current $K(\hat{p},\epsilon)$ for four momentum directions and integrated over the Fermi surface. With the domain wall the kernel $K(\epsilon,\hat{p}) < 1$ is suppressed due to Andreev reflection.

i.e., energy is not fully transmitted. This is interpreted as a partial Andreev reflection of incident quasiparticles from the spatially varying profile of the order parameter. Inserting Eq. (C2) into the heat current expression (19), we can express the conductance as

$$G = \int d\epsilon\, \epsilon\, \langle |\hat{p}_x|\, K(\epsilon,\hat{p})\rangle_{\hat{p}} \frac{\partial \Phi_0}{\partial T}\,, \tag{C4}$$

where the kernel $K(\epsilon,\hat{p})$ is

$$K(\epsilon,\hat{p}) = N_F v_F \frac{\left(1-\left|\gamma_0^R(\epsilon,\hat{p},x)\right|^2\right)\left(1-\left|\tilde{\gamma}_0^R(\epsilon,\hat{p},x)\right|^2\right)}{\left|1+\gamma_0^R(\epsilon,\hat{p},x)\tilde{\gamma}_0^R(\epsilon,\hat{p},x)\right|^2}\,. \tag{C5}$$

Again, because the energy flow is uniform, $K(\epsilon,\hat{p})$ does not depend on position x, even though γ_0^R does.

In Fig. 13 we plot the heat current kernel together with the density of states and the Andreev reflection length $1/\ell_\Delta = 2\,\mathrm{Im}[\gamma^R\tilde{\Delta}]/v_F$ appearing in Eq. (20). For uniform order parameter (dashed lines) $K(\epsilon,\hat{p}) = 1$ for $\epsilon > |\Delta(\hat{p})|$, and is zero for energies below the gap where there are no quasiparticle states. $\ell_\Delta(\epsilon,\hat{p})$ is finite for subgap states $\epsilon < \Delta(\hat{p})$, and infinite otherwise.

At the center of a domain wall, $\ell_\Delta(\epsilon > \Delta(\hat{p}),\hat{p},x)$ is finite (and can even be negative!) for the above-gap states, their spectral weight is moved into the ABS, and the amplitude of $K(\epsilon,\hat{p})$ is reduced, as shown by the solid lines in Fig. 13. In the clean limit, the conductance is reduced in the presence of a single domain wall, similar to a pinhole of perfect transparency [20].

[1] Y. Matsuda, K. Izawa, and I. Vekhter, J. Phys.: Condens. Matter **18**, R705 (2006).
[2] M. J. Graf, S.-K. Yip, J. A. Sauls, and D. Rainer, Phys. Rev. B **53**, 15147 (1996).
[3] B. Lussier, B. Ellman, and L. Taillefer, Phys. Rev. B **53**, 5145 (1996).
[4] M. R. Norman and P. J. Hirschfeld, Phys. Rev. B **53**, 5706 (1996).
[5] I. Vekhter and A. Vorontsov, Phys. Rev. B **75**, 094512 (2007).
[6] G. E. Volovik, Pis'ma v ZhETF **58**, 457 (1993) [JETP Lett. **58**, 469 (1993)].
[7] I. Vekhter, P. J. Hirschfeld, and E. J. Nicol, Phys. Rev. B **64**, 064513 (2001).
[8] M. Franz, Phys. Rev. Lett. **82**, 1760 (1999).
[9] I. Vekhter and A. Houghton, Phys. Rev. Lett. **83**, 4626 (1999).
[10] A. B. Vorontsov and I. Vekhter, Phys. Rev. B **75**, 224502 (2007).
[11] V. Mineev and K. Samokhin, *Introduction to Unconventional Superconductivity* (Gordon and Breach, New York, 1999).
[12] P. J. Hirschfeld, P. Wölfle, and D. Einzel, Phys. Rev. B **37**, 83 (1988).
[13] C. Capan, A. Bianchi, R. Movshovich, A. D. Christianson, A. Malinowski, M. F. Hundley, A. Lacerda, P. G. Pagliuso, and J. L. Sarrao, Phys. Rev. B **70**, 134513 (2004).
[14] S. Ryu, J. E. Moore, and A. W. W. Ludwig, Phys. Rev. B **85**, 045104 (2012).
[15] R. Nakai and K. Nomura, Phys. Rev. B **89**, 064503 (2014).
[16] B. Sothmann and E. M. Hankiewicz, arXiv:1603.08736.
[17] A. F. Andreev, J. Exptl. Theoret. Phys. **46**, 1823 (1964) [Sov. Phys. JETP **19**, 1228 (1964)]; J. Exptl. Theoret. Phys. **47**, 2222 (1964) [Sov. Phys. JETP **20**, 1490 (1965)].
[18] K. Maki, Phys. Rev. **158**, 397 (1967).
[19] U. Brandt, W. Pesch, and L. Tewordt, Z. Phys. **201**, 209 (1967).
[20] E. Zhao, T. Löfwander, and J. A. Sauls, Phys. Rev. Lett. **91**, 077003 (2003); Phys. Rev. B **69**, 134503 (2004).
[21] M. Eschrig, J. A. Sauls, and D. Rainer, Phys. Rev. B **60**, 10447 (1999).
[22] M. Eschrig, D. Rainer, and J. Sauls, in *Vortices in Unconventional Superconductors and Superfluids*, edited by R. Huebener, N. Schopohl, and G. Volovik, Springer Series in Solid-State Sciences, Vol. 132 (Springer, Berlin, Heidelberg, 2002), pp. 175–203.
[23] A. I. Larkin and Y. N. Ovchinnikov, Zh. Eksp. Teor. Fiz. **47**, 1136 (1964) [Sov. Phys. JETP **20**, 762 (1965)].
[24] H. Burkhardt and D. Rainer, Ann. Phys. **3**, 181 (1994).
[25] A. B. Vorontsov, J. A. Sauls, and M. J. Graf, Phys. Rev. B **72**, 184501 (2005).
[26] Y. Matsuda and H. Shimahara, J. Phys. Soc. Jpn. **76**, 051005 (2007).

[27] H. Mayaffre, S. Krämer, M. Horvatic, C. Berthier, K. Miyagawa, K. Kanoda, and V. F. Mitrović, Nat. Phys. **10**, 928 (2014).
[28] J. W. Serene and D. Rainer, Phys. Rep. **101**, 221 (1983).
[29] M. Eschrig, Phys. Rev. B **61**, 9061 (2000).
[30] A. V. Balatsky, I. Vekhter, and J.-X. Zhu, Rev. Mod. Phys. **78**, 373 (2006).
[31] A. C. Durst and P. A. Lee, Phys. Rev. B **62**, 1270 (2000).
[32] P. A. Lee, Phys. Rev. Lett. **71**, 1887 (1993).
[33] L. Taillefer, B. Lussier, R. Gagnon, K. Behnia, and H. Aubin, Phys. Rev. Lett. **79**, 483 (1997).